Warm Winter, Thin Ice?

Julienne Stroeve[1,2], David Schroder[3], Michel Tsamados[1], Daniel Feltham[3]

[1]Centre for Polar Observation and Modelling, Earth Sciences, University College London, London, UK
[2]National Snow and Ice Data Center, University of Colorado, Boulder, CO, USA
[3]Centre for Polar Observation and Modelling, Department of Meteorology, University of Reading, Reading, UK

Abstract

Winter 2016/2017 saw record warmth over the Arctic Ocean, leading to the least amount of freezing degree days north of 70°N since at least 1979. The impact of this warmth was evaluated using model simulations from the Los Alamos sea-ice model (CICE) and CryoSat-2 thickness estimates from three different data providers. While CICE simulations show a broad region of anomalously thin ice in April 2017 relative to the 2011-2017 mean, analysis of three CryoSat-2 products show more limited regions with thin ice and do not always agree with each other, both in magnitude and direction of thickness anomalies. CICE is further used to diagnose feedback processes driving the observed anomalies, showing 11-13 cm reduced thermodynamic ice growth over the Arctic domain used in this study compared to the 2011-2017 mean, and dynamical contributions of +1 to +4 cm. Finally, CICE model simulations from 1985-2017 indicate the negative feedback relationship between ice growth and winter air temperatures may be starting to weaken, showing decreased winter ice growth since 2012 as winter air temperatures have increased and the freeze-up has been further delayed.

Introduction

It is well known that Arctic air temperatures are rising faster than the global average [e.g. *Bekryaev et al.*, 2010; *Serreze and Barry*, 2011]. The thinning and shrinking of the summer sea ice cover have played a role in this amplified warming, which is most prominent during the autumn and winter months as the heat gained by the ocean mixed layer during ice-free summer periods is released back to the atmosphere during ice formation [e.g. *Serreze et al.*, 2009; *Screen and Simmonds*, 2010]. However, Arctic amplification has been found in climate models without changes in the sea ice cover [*Pithan and Mauritsen*, 2014]. Increased latent energy transport [*Graversen and Burtu*, 2016], the lapse rate feedback [*Pithan and Mauritsen*, 2014; *Graversen*, 2006] and changes in ocean circulation [*Polyakov et al.*, 2005] have also contributed. Furthermore, cyclones are effective means of bringing warm and moist air into the Arctic during winter [e.g. *Boisvert et al.*, 2016].

Winter 2015/2016 was previously reported as the warmest Arctic winter recorded since records began in 1950 [*Cullather et al.*, 2016]. Warming was Arctic-wide, with temperature anomalies reaching +5°C [*Overland and Wang*, 2016] and temperatures near the North Pole hitting 0°C [*Boisvert et al.*, 2016]. Part of the unusual warming was linked to a strong cyclone that entered the Arctic in December 2015 [*Boisvert et al.*, 2016], resulting in reduced thermodynamic ice growth and thinning within the Kara and Barents seas [*Ricker et al.*, 2017; *Boisvert et al.*, 2016]. This was one of several cyclones to enter the Arctic that winter as a result of a split tropospheric vortex that brought warm and moist air from the Atlantic Ocean towards the pole [*Overland and Wang*, 2016]. Winter 2016/2017 once again saw temperatures near the North Pole reach 0°C in December 2016 and February 2017 [*Graham et al.*, 2017]. These

47 warming events were similarly associated with large storms entering the Arctic [*Cohen et al.*,
48 2017]. It has been suggested that the recent warm winters represent a trend towards increased
49 duration and intensity of winter warming events within the central Arctic [*Graham et al.*, 2017].
50   In general, warm winters, combined with increased ocean mixed layer temperatures from
51 summer sea ice loss, delay freeze-up, impacting the length of the ice growth season and the
52 period for snow accumulation on the sea ice. *Stroeve et al.* [2014] previously evaluated changes
53 in the melt onset and freeze-up, showing large delays in freeze-up within the Chukchi, East
54 Siberian, Laptev and Barents seas, with delays increasing on the order of +10 days per decade.
55 Later freeze-up has a non-trivial influence on basin-wide sea ice thickness: ice grows
56 thermodynamically faster for thin ice than for thick ice [*Bitz and Roe*, 2004]. More subtle effects
57 involving the timing of ice growth relative to major snow precipitation events in fall have been
58 shown to also control the growth rate of sea ice thickness; ice grows faster for a thinner snow
59 pack [*Merkouriadi et al.*, 2017]. Nevertheless, the maximum winter sea ice extent in 2017 set a
60 new record low for the 3rd year in a row. Have the recent warm winters played a role in these
61 record low winter maxima by reducing winter ice formation?
62   *Ricker et al.* [2017a] previously evaluated the impact of the 2015/2016 warm winter on ice
63 growth using sea ice thickness derived from blending CryoSat-2 (CS2) radar altimetry with those
64 from Soil Moisture and Ocean Salinity (SMOS) radiometry [*Ricker et al.*, 2017b]. They found
65 anomalous freezing degree days (FDDs) between November 2015 and March 2016 within the
66 Barents Sea of 1000 degree days coincided with a thinning of approximately 10 cm in March
67 compared to the 6-year mean. While near-surface air temperatures largely control
68 thermodynamic ice growth, other processes also impact ice growth, including ocean circulation,
69 sensible and latent heat exchanges. Furthermore, winter ice thickness is not only a result of
70 thermodynamic ice growth, but rather the combined effects of thermodynamic and dynamic
71 processes. A thinner ice cover is more prone to ridging and rafting, as well as ice divergence,
72 leading to new ice formation within leads/cracks within the ice pack. This however was not
73 evaluated by *Ricker et al.* [2017a].
74   In this study we evaluate the impact of the 2016/2017 anomalously warm winter on Arctic
75 sea ice thickness using the Los Alamos sea-ice model (CICE) [*Hunke et al.,* 2015] and satellite-
76 derived CS2 thickness data from three different sources: Centre for Polar Observation and
77 Modeling (CPOM) [*Tilling et al.*, 2017], Alfred Wegener Institute (AWI) [*Hendricks et al.*,
78 2016], and NASA [*Kurtz and Harbeck*, 2017]. CICE is initialized with CPOM CS2 sub-grid
79 scale ice thickness distribution (ITD) fields in November and run forward with NCEP
80 Reanalysis-2 (NCEP2) atmospheric reanalysis data [*Kanamitsu et al.*, 2002, updated 2017]. The
81 model run is subsequently compared over the winter growth season to CS2 thickness from the
82 three different data providers and contributions of thermodynamics vs. dynamics to the thickness
83 anomalies are evaluated. While the focus is on the 2016/2017 ice growth season, a secondary
84 aim is to compare existing CS2 products to inform the community on uncertainties in these
85 estimates and inform on model limitations. Thus, results are also presented for other years during
86 the CS2 time-period for comparison. To our knowledge, this is the first study to compare
87 different CS2 data products over the lifetime of the mission.
88
89 **Methods**
90 *Ice Thickness Distribution (ITD) from Cryosat-2*
91   The CryoSat-2 radar altimetry mission was launched April 2010, providing estimates of ice
92 thickness during the ice growth season. CS2 provides freeboard estimates, or the height of the ice

93 surface above the local sea surface, which when combined with information on snow depth,
94 snow density and ice density can be converted to ice thickness assuming hydrostatic equilibrium
95 [e.g. *Laxon et al.*, 2013]. Here we evaluate ice thickness fields provided by three different data
96 providers in order to assess robustness of the observed thickness anomalies. Thickness is
97 retrieved from ice freeboard by processing CS2 Level 1B data, with a footprint of 300m by
98 1700m, and assuming snow density and snow depth from the *Warren et al.* [1999] climatology
99 (hereafter *W99*), modified for the distribution of multiyear versus first-year ice (i.e. snow depth
100 is halved over first-year ice) [see *Laxon et al.*, 2013 and *Tilling et al.*, 2017 for data processing
101 details].
102   While the three data providers rely on *W99* for snow depth and density, each institution
103 processes the radar returns differently. In general, the range to the main scattering horizon of the
104 radar return is obtained using a retracker algorithm. This can be based on a threshold [e.g *Laxon*
105 *et al.*, 2013; *Ricker et al.*, 2014; *Hendricks et al.*, 2016], or a physical retracker [*Kurtz et al.*,
106 2014]. While the CPOM and AWI products use a leading edge 70% threshold retracker, *Kurtz*
107 *and Harbeck* [2017] rely on a physical model to best fit each CryoSat-2 waveform. This will lead
108 to ice thickness differences based on different thresholds applied: *Kurtz et al.* [2014] found a 12
109 cm mean difference between using a 50% threshold and a waveform fitting method.
110   We note that several factors contribute to CS2-derived sea ice thickness uncertainties,
111 including the assumption that the radar return is from the snow/ice interface [*Willat et al.*, 2011],
112 snow depth departures from climatology and the use of fixed snow and ice densities. In this
113 study we initialize the CICE model simulations described below with the CPOM sea ice
114 thickness fields. Accuracy of the CPOM product has been evaluated in several studies,
115 suggesting mean biases between thickness observations in 2011 and 2012 of 6.6 cm when
116 compared with airborne EM data [*Laxon et al.*, 2013; *Tilling et al.*, 2015]. For April 2017, the
117 CPOM near-real-time product [*Tilling et al.*, 2016] was used in place of the archived product,
118 with a mean thickness bias of 0.9 cm between these products.
119   In this study, individual thickness point measurements are binned into 5 CICE thickness
120 categories (1: < 0.6m, 2: 0.6-1.4m, 3: 1.4-2.6m, 4: 2.6-3.6m, 5: > 3.6m) on a rectangular 50km
121 grid for each month. The mean area fraction and mean thickness is derived for each thickness
122 category and these values are interpolated on the tripolar 1 degree CICE grid (~40km grid
123 resolution). Grid points with less than 100 individual measurements and a mean SIT < 0.5 m are
124 not included. Otherwise, all individual observations are included. For November, this effectively
125 limits the area of the Arctic to the region shown in Figure 1(c). Negative thickness values that are
126 retained in the CS2 processing to prevent statistical positive bias of the thinner ice are added to
127 category 1. The novel approach of initializing the CICE model with the full ITD rather than the
128 mean sea ice thickness provides an additional control on the repartition of the ice among
129 different thickness categories. This in turn allows a more accurate representation of ice growth
130 and ice melt processes [*Tsamados et al.*, 2015] compared to initializing with the mean grid-cell
131 SIT and deriving the fractions for each ice category assuming a parabolic distribution. Ice growth
132 and melt strongly depend on SIT: using a real distribution can have a big impact, especially for
133 thin ice.

134 *CICE Simulations*
135   CICE is a dynamic-thermodynamic sea-ice model designed for inclusion within a global
136 climate model. The advantages of using CICE for this study is that we can more readily separate
137 thickness anomalies into their thermodynamic and dynamical contributions, examine inter-

138 annual variability and perform longer simulations. For this study, we performed two different
139 CICE simulations. The first is a multiyear simulation from 1985 to 2017 (referred to as CICE-
140 free). The second is a stand-alone sea-ice simulation for the pan-Arctic region starting in mid-
141 November and running until the end of April of the following year for the last 7 winter periods
142 from 2010/2011 to 2016/2017. This results in seven 1-year long simulations (referred to as
143 CICE-ini), in which the initial thickness and concentration for each of the 5 ice categories is
144 updated from the CS2 ITD using the CPOM CS2 November thickness fields. For grid points
145 without CS2 data, and for all other variables (e.g. temperature profiles, snow volume), results
146 from the free CICE simulation with the same configuration started in 1985 are applied. In this
147 way, CICE simulations cover the pan-Arctic region, but in regions where no CS2 are available,
148 we restart SIT values from the free CICE model run. While this approach would be problematic
149 in a coupled model, in a stand-alone sea ice simulation the model adjustment to the new
150 conditions is smooth and the impact of using the vertical temperature profile from the free
151 simulation only affects sea ice thickness on the order of millimeters.
152   Snow accumulation can depart strongly from the *W99* climatology for individual years. Thus,
153 we make the assumption that the deviation of the mean *annual* cycle of snow depth over the last
154 7 years from the *W99* climatology is small and assume mean winter ice growth to be determined
155 accurately from CS2, and tuned CICE-ini accordingly to match the observed CS2 mean winter
156 ice growth from the CPOM product in the central Arctic [**Figure 1**]. The excellent agreement for
157 both CICE-ini and CICE-free with CS2 increases the confidence of our model results. Our
158 approach therefore allows us to study inter-annual variability from 2 model configurations with
159 different sources of errors, in addition to the 3 CS2-based products.
160   For both CICE simulations, NCEP-2 provides the atmospheric forcing. We use NCEP-2 2m
161 air temperatures because they have been shown to be more realistic for the Arctic Ocean than
162 those from ERA-Interim [*Jakobshavn et al.*, 2012]. The setup is the same as described *in*
163 *Schröder et al.* [2014] including a simple ocean-mixed layer model, a prognostic melt pond
164 model [*Flocco et al.*, 2012] and an elastic anisotropic-plastic rheology [*Tsamados et al.*, 2013],
165 with the following improvements: we apply an updated CICE version 5.1.2 with variable
166 atmospheric and oceanic form drag parameterization [*Tsamados et al.* 2014], we increase the
167 thermal conductivity of fresh ice from 2.03 W/m/k to 2.63 W/m/K, snow from 0.3 W/m/K to 0.5
168 W/m/K and the emissivity of snow and ice from 0.95 to 0.976. While the default conductivity
169 values are at the lower end of the observed range, the new values are at the upper end and have
170 been applied in previous climate simulations [e.g. *Rae et al.*, 2014].
171   Below, all CS2-derived sea ice thickness anomalies are computed relative to the CS2 time-
172 period: November anomalies are relative to 2010-2016, and for April they are relative to 2011-
173 2017. Results for November and April are only shown for all grid cells which have a minimum
174 thickness of 50 cm and a minimum of 100 individual measurements for each of the seven years.
175 For the month of November, this corresponds to all colored area shown in Figure 1(c). For April,
176 this region represents the area in red shown in Figure 1(d). The larger region shown in Figure
177 1(d) also corresponds to the region over which the amount of thermodynamic ice growth and
178 dynamical ice growth between November and April are assessed from the CICE simulations. For
179 comparison with CS2, we present the mean thickness of the ice-covered area. In winter, the sea
180 ice concentration in the model generally ranges between 0.98 and 0.995% apart from locations
181 close to the ice edge. Further note that area-averaged values for November and April are only
182 given for regions shown in Figure 1(c) and Figure 1(d), respectively.
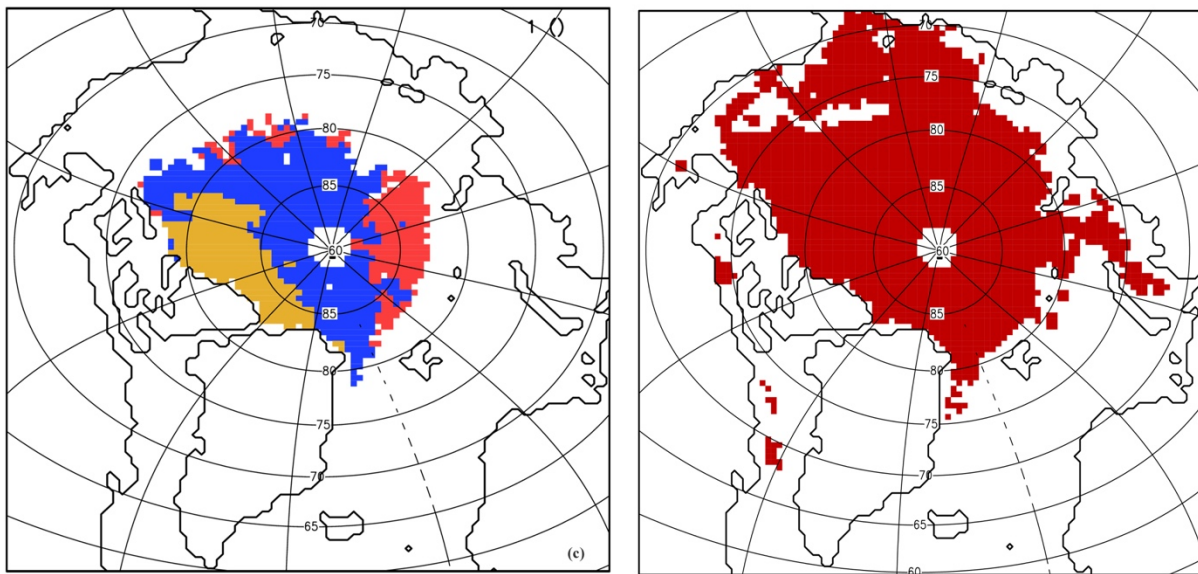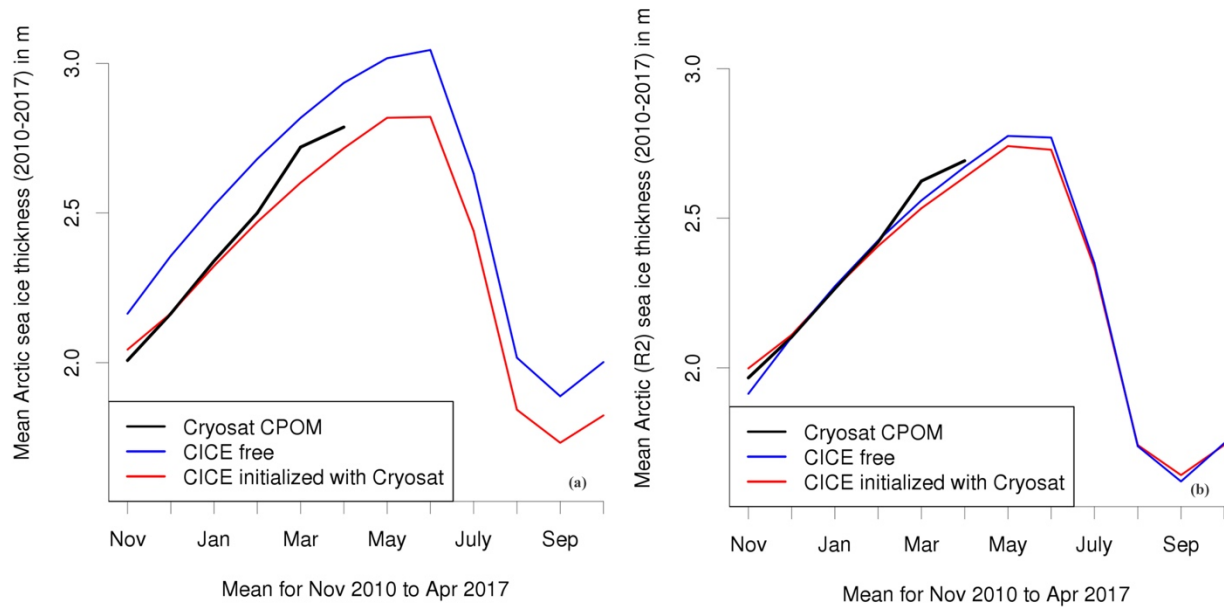
183
184 **Figure 1.** Comparison of CPOM CryoSat-2 mean seasonal sea ice thickness (black) with CICE free (blue) and CICE
185 initialized with Cryosat-2 in November (red). Figure 1(a) shows results for mean thickness averaged over all the
186 colored areas shown Figure1(c), representing the total region for which Cryosat-2 data exist in November (only grid
187 points included with > 100 measurements per month and mean thickness > 0.5m) and (b) mean thickness averaged
188 over the sub-region shown in blue with medium thick ice in January (between 1.5 and 2.5m). Blue areas in Figure
189 1(c) show regions between November and January where CryoSat-2 thickness are between 1.5 and 2.5 m in all
190 years; red for thin ice (< 1.5) and orange for thick ice (> 2.5m). Figure 1(d) is the region over which the April
191 thickness anomalies and results are presented.

192

193 **Results**
194 *Air temperature and freezing anomalies*
195   The growing season air temperatures anomalies (i.e. mid-November 2016 to mid-April 2017
196 relative to 1981-2010) were positive throughout the Arctic, leading to large reductions in the
197 number of FDDs, computed as the cumulative daily 2 m NCEP-2 air temperatures below -1.8°C,

198 similar to *Ricker et al.* [2016]. FDDs computed this way reflect both the number of days with air
199 temperatures below freezing, and the magnitude of below freezing air temperatures over the
200 specified period. Spatially, FDD anomalies show widespread reductions over most of the Arctic
201 Ocean, with the largest reductions in the Barents and Kara seas, stretching across the pole
202 towards the Beaufort and Chukchi seas [**Figure 2b**]. In contrast, during winter 2015/2016, FDDs
203 were most notably anomalous within the Barents and Kara seas [**Figure 2a**], in agreement with
204 *Ricker et al.* [2017a]. Overall, as averaged from 70-90°N, this past winter witnessed the least
205 amount of cumulative FDDs since at least 1979 [**Figure 2c**].
206
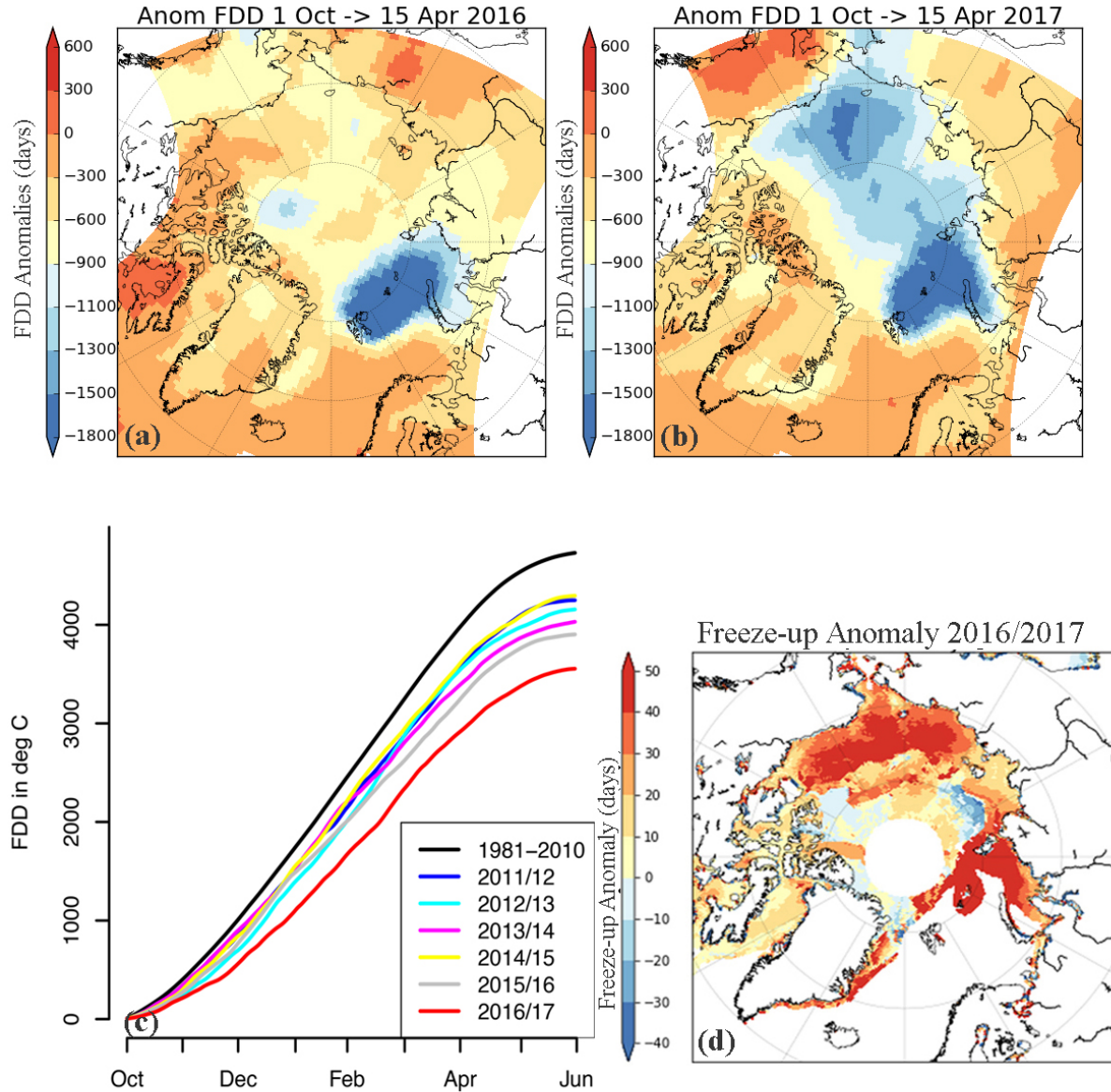
207
208 **Figure 2.** Top panel shows the freezing degree anomalies (FDD) computed as the number of days with NCEP2 2m
209 air temperature below -1.8°C from mid-November to mid-April in winter 2016 (a) and winter 2017 (b) computed
210 relative to the 1981-2010 climatology. Bottom left image shows the cumulative freezing degree days (FDDs)
211 averaged over region shown in Figure 3 inset (c), and bottom right image shows freeze-up anomalies for 2016/2017
212 relative to 1981-2010 (d). Areas in white are either missing (pole hole) or no sea ice in winter 2016/2017.

213   While ice forms quickly within the central Arctic once air temperatures drop below freezing, this
214   year saw large delays in freeze-up throughout the Arctic. Updating results previously reported in
215   *Stroeve et al*. [2014], freeze-up was delayed by 20 days for the Arctic as a whole, with regions
216   like the Bering, Beaufort, Chukchi, East Siberian and Kara seas delayed by three to four weeks
217   [**Figure 2d**]. Within the Barents Sea, the regionally averaged freeze-up was delayed by 60 days.
218   In recent years, the trend towards later freeze-up has increased, with the Barents and Chukchi
219   seas showing the largest trends on the order of +14 days per decade through 2017, followed by
220   the Kara and East Siberian seas with delays on the order of +10 to +12 days per decade. Within
221   the Beaufort Sea, freeze-up is now happening later by +9 days per decade [**Table 1**].
222
223   ***November ice thickness anomalies***
224   Before analyzing how the reduced number of freezing degree days impacted winter ice
225   growth during 2016/2017, it is useful to first inter-compare the different CryoSat-2 thickness
226   estimates. We start with a comparison of November thickness from the three CS2 data sets from
227   November 2010 to 2016 [**Figure 3**]. It is encouraging to find that year-to-year variability in the
228   spatial patterns of positive and negative thickness anomalies are generally consistent between the
229   three products despite differences in waveform processing. The AWI and CPOM data sets are in
230   better agreement with each other than with the NASA product, which is expected as they use a
231   similar retracker. Furthermore, all three data sets show widespread thinner ice in November
232   2011, and widespread thicker ice in November 2013. This is further supported by analysis of
233   regional mean thickness and anomalies computed over the region shown in Figure 1(c) [**Table
234   2**]. For comparison, we also list results from the CICE-free model simulation. In November
235   2011, the different CS2 data products are in agreement that the ice was anomalously thin (-32 to
236   -46 cm), the thinnest in the CS2 data record. Similarly, in November 2013, all three CS2
237   products show overall thicker ice on the order of +23 to +38 cm. The CICE-free simulations also
238   show anomalously thinner and thicker ice during these years, but larger anomalies were
239   simulated in 2012 and 2014.
240   While the overall pattern of years with anomalously thin or thick ice is broadly similar
241   between the three CS2 products, this is not true in 2016. Both the CPOM and AWI thickness
242   estimates suggest slightly thicker ice than average (+4 cm and +9 cm, respectively), while the
243   NASA product suggests the icepack was overall slightly thinner (-1 cm). The CICE-free run is in
244   agreement with the NASA data set for the 2016 anomaly. Turning back to **Figure 3**, we find that
245   in 2016 the CPOM data set shows +20 to +60 cm thicker ice north of the Canadian Archipelago
246   (CAA) and Greenland, -20 to -60 cm thinner ice on the Pacific side of the pole, and +10 to +30
247   cm thicker ice north of the Laptev Sea. These spatial patterns of November 2016 SIT anomalies
248   are broadly similar with those from AWI but less so with NASA. However, despite similar
249   patterns of positive and negative thickness anomalies, AWI shows between +20 and +30 cm
250   thicker ice over much of the central Arctic Ocean, and even thicker ice (up to +60 cm) north of
251   the CAA and Greenland in November 2016 than the CPOM product. NASA on the other hand
252   shows larger negative anomalies on the Pacific side of the north pole of up to -70 cm and larger
253   positive anomalies directly north of the CAA between +10 and +20 cm.
254   Since we use CPOM CS2 thickness fields to initialize our CICE model runs, this comparison
255   is useful in determining whether or not the 2016 November thickness anomalies are robust in
256   other CS2 processing streams and provides a measure of CS2 sea ice thickness uncertainty.
257   However, since we do not have the AWI and NASA ITDs we cannot quantify the impact of
258   using a different thickness data set on our simulations. However, as a result of the negative
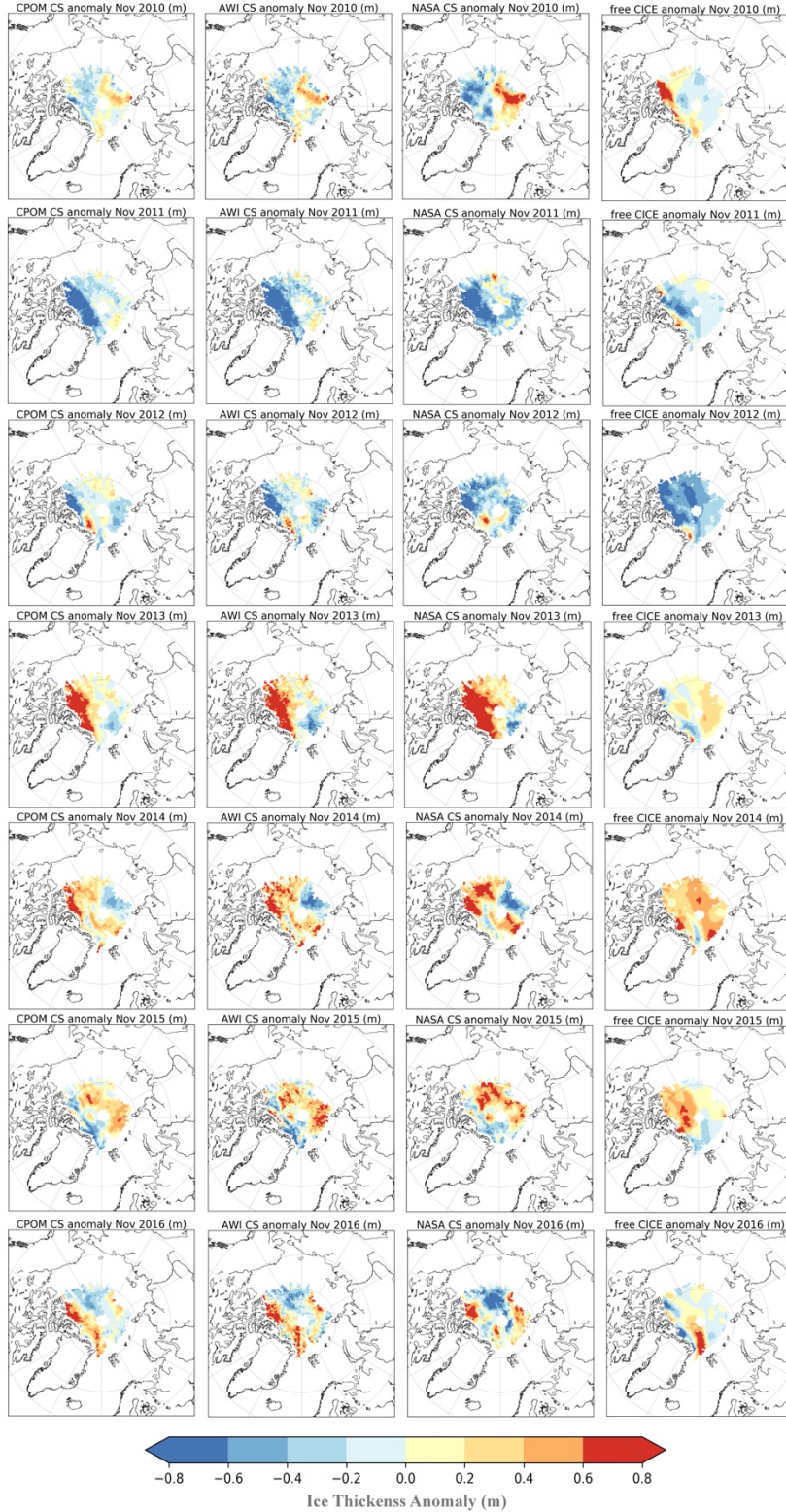
259
260 **Figure 3**. November ice thickness anomaly relative to 2010-2016 in cm based on CryoSat-2 data from UCL CPOM
261 (left), Alfred Wegener Institute (AWI) (middle) and NASA (right). Grid points with less than 100 individual
262 measurements and a mean sea ice thickness of less than 0.5 m are not included. CICE-free thickness anomalies are
263 also shown in the left right column.

264 winter ice growth feedback (discussed below), differences due to model initialization in
265 November will be attenuated until April.
266
267 ***Sea Ice growth from November to April***
268   For a more robust analysis of winter ice growth during the record warm winter of 2016/2017,
269 we now include April thickness estimates from CS2 (CPOM, AWI and NASA), the free CICE
270 simulation and the CICE simulations initialized with CPOM CS2 November SIT in **Figure 4**.
271 Corresponding values for all other years are shown in **Figure 5** (CS2) and **Figure 6** (CICE).
272 **Table 3** summarizes associated mean April thickness and anomalies since 2011, together with
273 contributions from thermodynamics (ice growth) and dynamics (ice transport and ridging) based
274 on the CICE model simulations. The area for which these estimates are provided corresponds to
275 the area shown in Figure 1(d).
276   We first note that all 5 estimates have different strengths and weaknesses: while the mean
277 annual cycle of sea ice thickness *should* be more accurate from CS2 than modeled estimates,
278 robust analysis of winter ice growth from CS2 is in part limited due to the impact of
279 climatological snow depth assumptions, which may differ from one year to the next, and
280 differences in waveform processing between CS2 data providers, which may result in
281 inconsistencies in the magnitude and direction of the observed thickness anomalies. In the free
282 CICE simulation, November sea ice thickness is less certain due to error accumulation during the
283 model run. In the initialized CICE simulation, both these error sources are reduced but inherent
284 model biases remain. While the thermodynamic ice growth can be regarded as quite accurate in
285 CICE (error of April ice thickness around 10-20cm), uncertainty caused by dynamics
286 (divergence, ridging) can be larger under certain conditions. Below we discuss some of the
287 regional differences, but we are most confident in the model simulations on the Arctic Basin-
288 wide scale over which CICE has been tuned to agree with CS2 winter ice growth.
289   Despite these limitations, all five approaches show good agreement in most years regarding
290 the direction of the thickness anomalies (i.e. positive or negative) even if they disagree on
291 absolute magnitude. For example, Arctic Ocean mean thickness anomalies are negative in all 3
292 CS2 products for April 2013 (ranging from -3 to -25 cm), whereas in April 2014 and 2015 all
293 approaches give positive mean thickness anomalies, ranging from +5 to +20 cm in 2014 and +11
294 to +22 cm in 2015 [**Table 3**]. In some years, the CICE-free simulation better matches the
295 observed April thickness anomalies (e.g. 2013, 2015), whereas in other years CICE-ini performs
296 better (e.g. 2012, 2014). On the other hand, in 2011 and 2017 we find disagreement among the
297 three CS2 data sets. In April 2011, both the CPOM and NASA product have overall negative
298 thickness anomalies for the Arctic Basin (-4 and -8 cm, respectively), whereas they are positive
299 in the AWI product (+7 cm). In April 2017, both the CPOM and AWI are in close agreement that
300 the ice cover was overall thinner (-13 and -12 cm, respectively), as are the CICE-free and CICE-
301 ini simulations (negative thickness anomalies of -13 cm), whereas NASA shows a weak positive
302 anomaly (+3cm).
303   Focusing more on April 2017, the 3 CS2 products suggest widespread thinner ice in April
304 2017 north of Ellesmere Island (up to -80 cm thinner) relative to the 2011-2017 mean [**Figure**
305 **4(top)**]. Thinner ice is also found within the Chukchi and East Siberian seas (on average -10 to -
306 35 cm thinner) despite a mix of positive and negative anomalies. CICE simulations on the other
307 hand show more widespread thinning throughout the western Arctic, including the Beaufort Sea
308 and positive thickness anomalies north of Ellesmere Island **[Figure 4(middle and bottom)]**. In
309 the Beaufort Sea, there is general disagreement among the 3 CS2 products as well as with the

310   CS2 results and the CICE simulations: regional mean anomaly of -5 cm (CPOM), 0 cm (AWI),
311   +20 cm (NASA), -25 cm (CICE-ini) and -30 cm (CICE-free). North of Ellesmere Island, CICE-
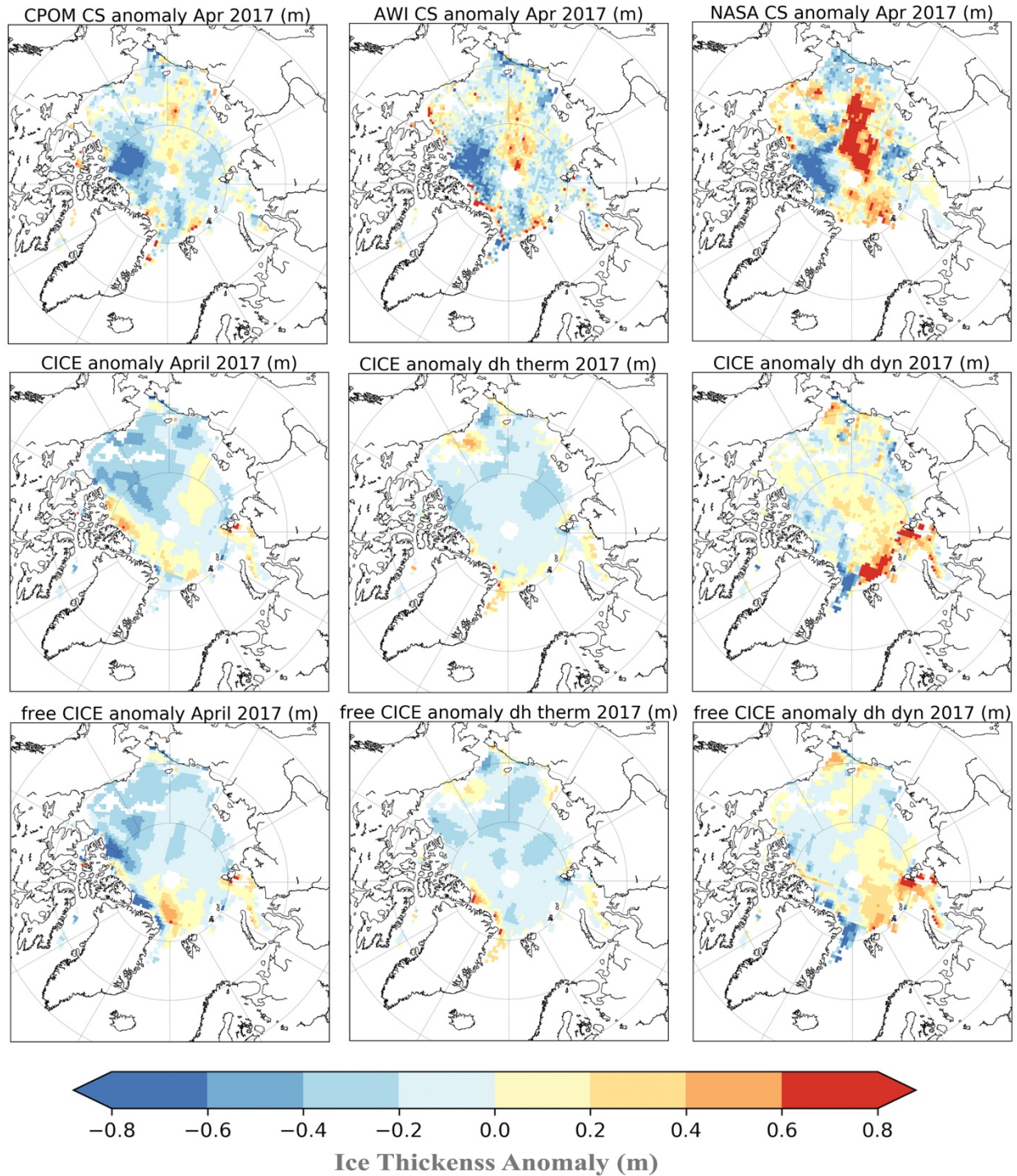
312
313   **Figure 4.** CryoSat-2 and CICE simulated thickness anomalies in April 2017 relative to the 2011-2017 mean. Top
314   images show the total ice thickness anomalies from CryoSat-2 for CPOM (left), AWI (middle) and NASA (right).
315   The middle left image shows April 2017 thickness anomalies from CICE initialized with CPOM November CS2
316   thickness together with the contributions from thermodynamics (middle) and dynamics (left) and bottom show the
317   corresponding results from the CICE free simulations. Grid points with less than 100 individual measurements and a
318   mean sea ice thickness of less than 0.5 m are not included.
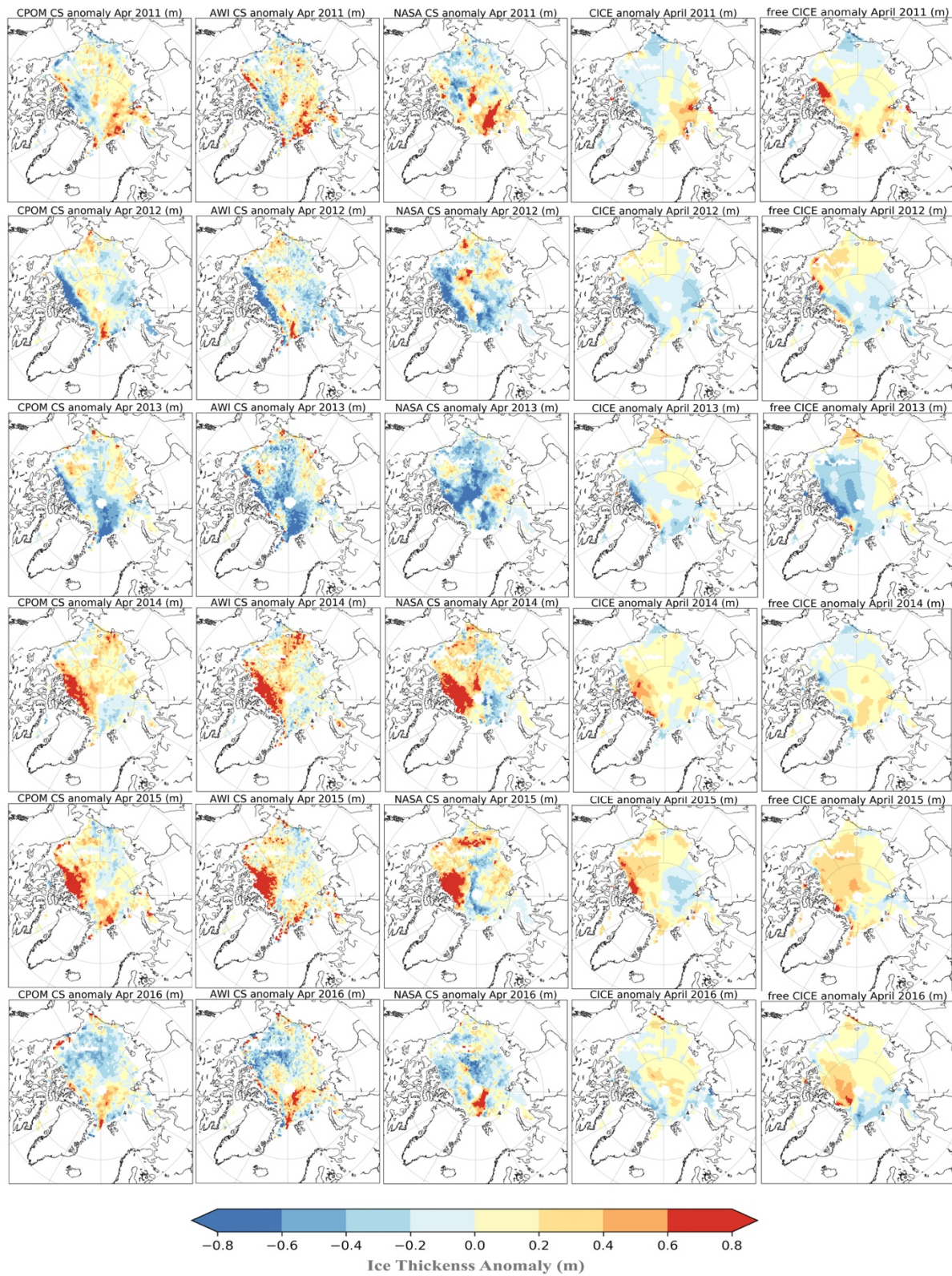
319
320 **Figure 5.** Anomaly of April ice thickness from 2011 to 2016 in m relative to the 2011 to 2017 mean from CryoSat-2
321 CPOM (far left), AWI (second left), NASA (middle), CICE simulations initialized with November CPOM CryoSat-
322 2 thickness fields (2nd right), and CICE simulations not initialized with CryoSat-2 thickness (right). Grid points with
323 less than 100 individual measurements and a mean sea ice thickness of less than 0.5 m are not included.

324
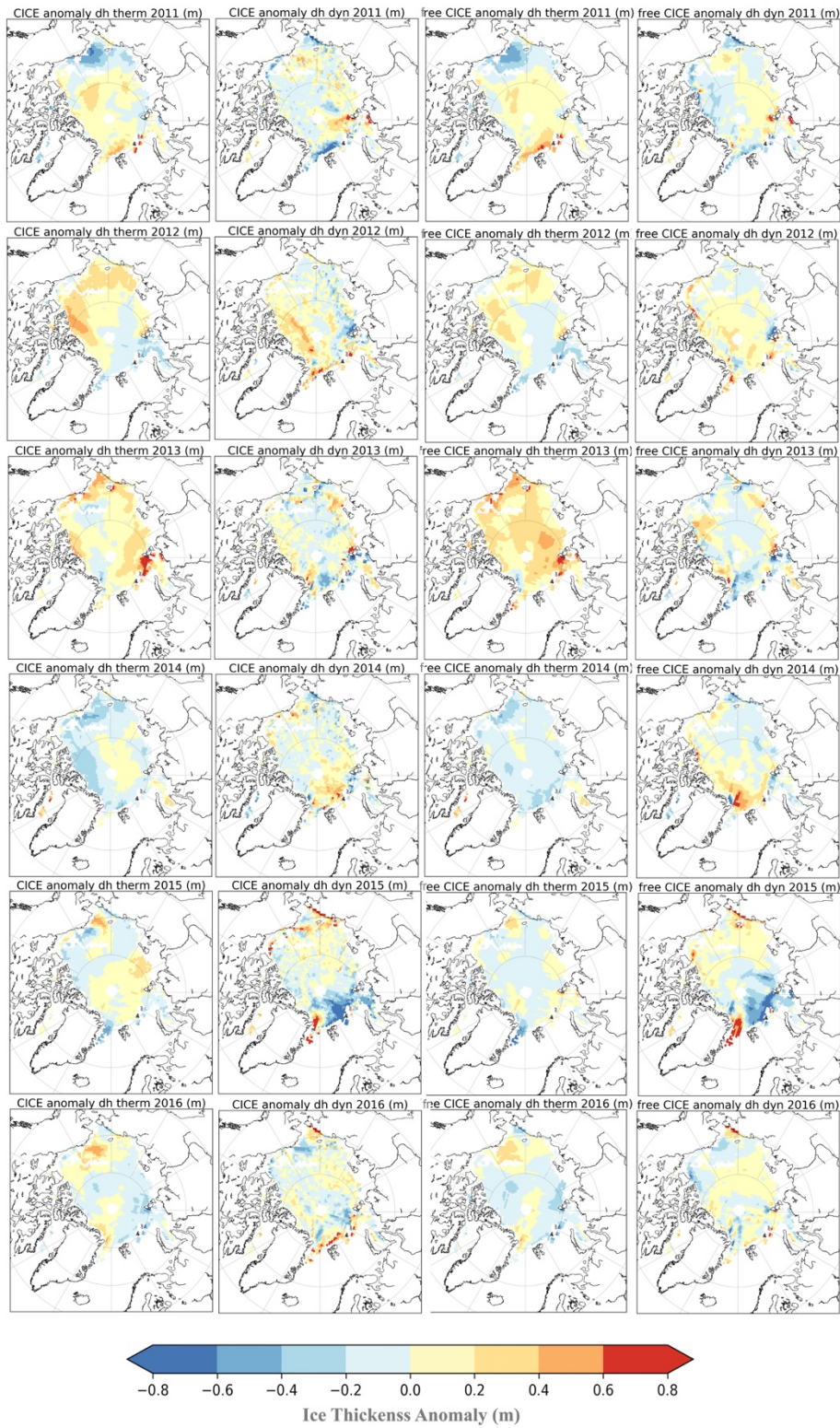
325
326 **Figure 6.** Anomalies of CICE simulated thermodynamic ice growth and dynamical thickness changes in m relative
327 to the 2011 to 2017 mean from the CICE simulations initialized with November CPOM CryoSat-2 thickness fields
328 (left), and CICE simulations not initialized with CryoSat-2 thickness (right). The year in title reflects the end month
329 over which ice growth occurs (e.g. from November to April).

330
331 ini indicates positive thickness anomalies (up to +50 cm), whereas all 3 CS2 products show
332 negative thickness anomalies (up to -80 cm). In this region, the CICE-free simulation also shows
333 mostly negative thickness anomalies (-20 to -80 cm), with a small positive area (up to +25 cm).
334   While the discrepancy in this region is puzzling, the bias between the CICE-ini simulations
335 and the CS2 products may in part reflect the use of a snow climatology in the CS2 thickness
336 retrievals. As discussed earlier, a positive sea ice thickness anomaly was found in the November
337 2016 CS2 thickness retrievals north of CAA and Greenland. Yet this positive thickness anomaly
338 is not preserved through April in both the CPOM and AWI CS2 products. **Figure 7** shows CICE
339 simulated snow depth anomalies in November 2016 and April 2017. In November, small positive
340 snow depth anomalies occur throughout the Arctic, especially north of the Queen Elizabeth
341 Islands where the anomaly locally increases to 20 cm. By April, the anomalies cover a broader
342 region and increase in magnitude. A positive April snow depth anomaly of 15 to 20 cm relative
343 to *W99* would result in an underestimation of the CS2-retrieved April ice thickness (SIT) by 88
344 to 115 cm using the following equation:
345

$$SIT = \frac{\rho_{snow}H_{snow} + \rho_{water}F_c}{(\rho_{water} - \rho_{ice})}$$

346

347
348 where F_c is the corrected radar freeboard (F_b) for the reduced propagation of the speed of light
349 through the snow cover ($F_c = F_b + 0.25H_{snow}$) [*Tilling et al.*, 2017], and using a snow density
350 (ρ_{snow}) of 320 kg/m^3 [*Warren et al.*, 1999], ice density (ρ_{ice}) of 915 kg/m^3, water density of
351 (ρ_{water}) 1024 kg/m^3. CICE-ini, which relies on the CPOM CS2 November thickness, maintains
352 this positive thickness anomaly through April despite reduced thermodynamic ice growth. While
353 it is difficult to ascertain the accuracy of the CICE snow depths, comparison with snow depths
354 collected by *Haas et al.* (2017) in the Lincoln Sea showed CICE snow depths were
355 underestimated on average by 10cm (not shown). Thus, the overall impact on overall ice
356 thickness may be less than computed here. The CICE-free simulation on the other hand started
357 with negative thickness anomalies in November within this region, and maintains them through
358 April.
359
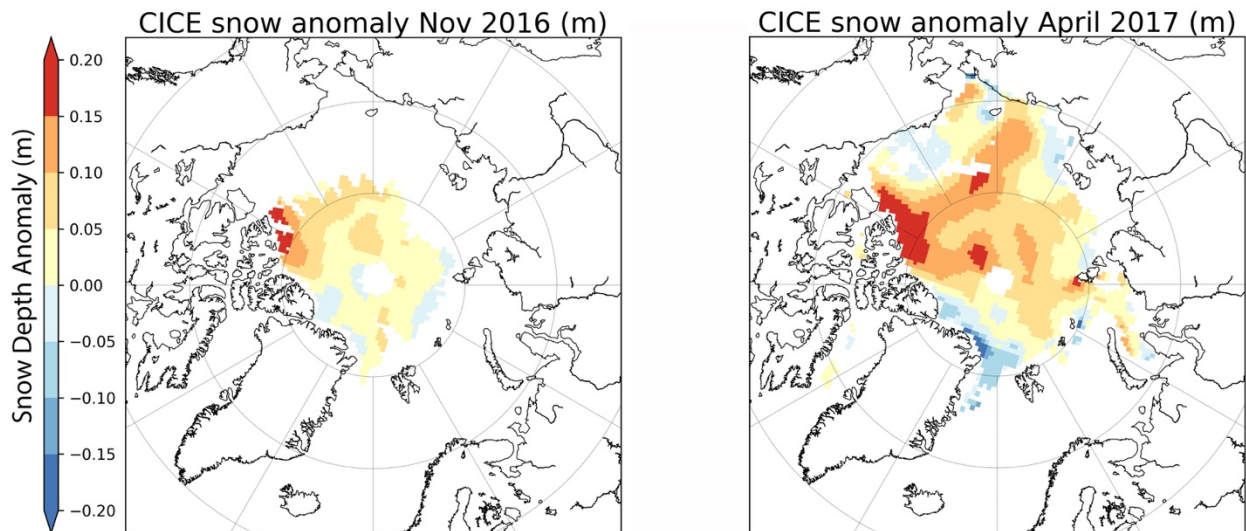
360

On the other hand, thickness is also strongly influenced by dynamics, such as convergence against the CAA and Greenland which leads to thicker ice in this region [*Kwok et al.*, 2015]. During winter 2017 however, the Beaufort High largely collapsed [*Moore et al.,* 2018], reducing convergence against the northern CAA and Greenland [**Figure 8**]. One advantage of using CICE, is that we can more readily diagnose thermodynamic vs. dynamical contributions to the observed thickness anomalies. For the region directly north of Ellesmere Island, both the CICE-ini and CICE-free simulations support reduced sea ice convergence, leading to thinner ice from dynamical contributions. At the same time, this region also exhibited reduced thermodynamic ice growth in both CICE simulations. One would expect thermodynamic ice growth to be reduced in regions of enhanced snow depth and thicker November ice. Positive snow depth anomalies extended from this region through the northern Beaufort Sea, in agreement with extended regions reductions in thermodynamic ice growth in both CICE-free and CICE-ini. At the same time, regions of positive 2016 November thickness anomalies are also associated with regions of reduced CICE thermodynamic ice growth.

Overall, the largest reductions in thermodynamic ice growth during winter 2016/2017 occurred within the Chukchi Sea and north of the CAA, extending through the northern Beaufort Sea (on the order of -40 cm). While snow depth and thickness anomalies influenced thermodynamic ice growth north of the CAA, within the Chukchi Sea the negative ice growth anomalies was a result of late ice formation: ice formed a month later than the 1981-2010 mean within the Chukchi Sea. This seems to have been more important than increases in ice thickness from dynamics. Dynamical thickness changes simulated by CICE show an overall thickening of the ice in winter 2016/2017 within the Chukchi and Bering seas (up to 50 cm). Anomalous ridging in this region is in agreement with observed high amounts of deformation along the shore fast ice zone within the Chukchi Sea as a result of persistent west winds from December to March (http://arcus.org/sipn/sea-ice-outlook/2017/june).

An exception to reduced thermodynamic ice growth occurs directly north of Utqiaġvik, Alaska (formerly Barrow), with positive thermodynamic ice growth anomalies of 30 to 40 cm. This enhanced ice growth was offset by ice divergence, leading to overall thinner ice in the CICE simulations. *In situ* observations of level first-year ice thickness off the coast of Utqiaġvik ranged between 1.35 and 1.40m during May (http://arcus.org/sipn/sea-ice-outlook/2017/june) and appear to be in better agreement with the CICE simulations, as well as the CPOM and AWI CS2 thickness estimates, while the NASA CS2 product shows positive thickness anomalies in that region. Positive thermodynamic ice growth anomalies are also found for small regions north of Greenland and within Fram Strait, as well as within some scattered coastal regions of the Chukchi, East Siberian, Laptev and Kara seas.

Finally, large dynamical thickening was found within the Kara and northern Barents seas (up to 1.2 m) and to a lesser extent over the southern and western Greenland Sea, Baffin Bay and the Labrador Sea (not shown). The CICE-simulated dynamical thickening in the Barents and Kara seas is more anomalous than seen during previous CS2 years [**Figure 6**], and likely reflects the influence of the positive Arctic Oscillation (AO) on ice motion [**Figure 8**]. The AO was positive from December through March, a pattern which results in offshore ice advection from Siberia and enhanced ice advection through Fram Strait [*Rigor et al.*, 2002]. This pattern leads to development of thin ice in newly formed open water areas, increasing thermodynamic ice growth in the Laptev Sea, whereas increased ice advection from thick ice regions north of Greenland

408   towards Fram Strait, combined with changes in internal ice stress as the ice cover has thinned,
409   leads to more deformation. Interestingly, while the CICE model runs confirm overall slightly
410
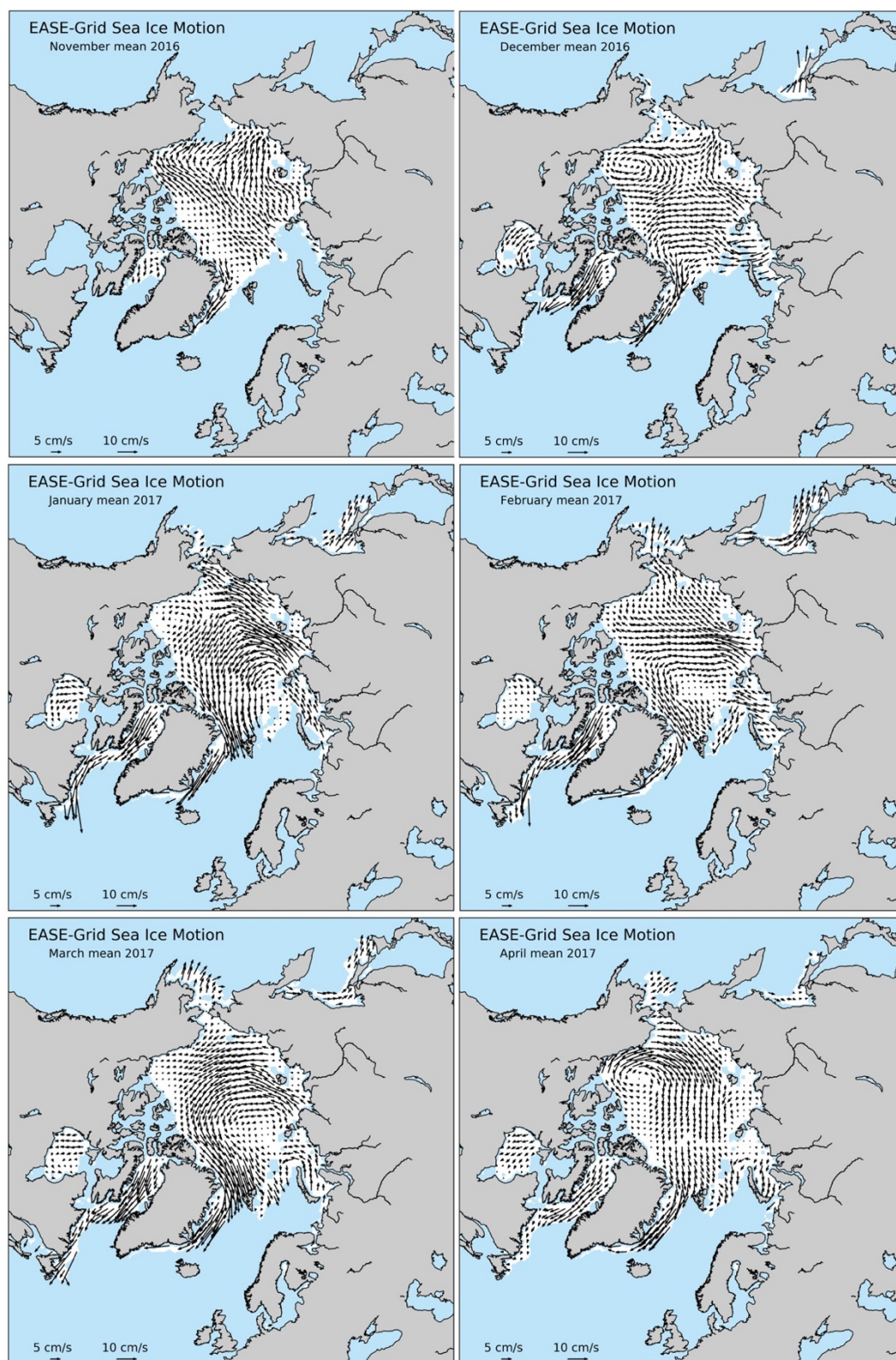
411
412 **Figure 8.** Mean monthly sea ice motion from the NSIDC Polar Pathfinder Data Set. Preliminary data provided by
413 Scott Stewart, NSIDC.
414

415 thinner ice within the Barents Sea in April 2016, consistent with the studies by *Ricker et al.*
416 [2017a] and *Boisvert et al.* [2016], the thinning from reduced thermodynamic ice growth was
417 largely offset by thickening from dynamical effects [**Figures 5 and 6**].
418   Overall, for the Arctic Basin as a whole, CICE simulations suggest the overall thinner ice
419 observed in April 2017 is largely result of reduced thermodynamic ice growth (-11 to -13 cm),
420 with dynamics adding +1 to +4 cm [**Table 3**].
421
422 *Negative feedbacks*
423   Ice growth after the September minima is a result of turbulent heat flux exchanges between
424 the relatively warm ocean mixed layer and the cold autumn and winter air through the snow-
425 covered sea ice. Progressively, as the ice grows to about 1.5 to 2 m thick, the ocean becomes
426 well insulated from the atmosphere and ice growth is slowed. Thus, it is not surprising that we
427 see less thermodynamic ice growth in regions of relatively thick (> 2.5 m) November ice. A case
428 in point is seen in winter 2013/2014 when thermodynamic ice growth was reduced by 9 to 10
429 cm, despite an overall colder winter.
430   On the other hand, thinner ice regions generally exhibit more vigorous ice growth. For
431 example, during winter 2012/2013, CICE-free, and to a lesser extent CICE-ini simulated
432 thermodynamic ice growth increased throughout much of the Arctic Ocean in areas where the ice
433 retreated in September 2012 [**Figure 6**] and where the November 2012 thickness anomalies were
434 negative [**Figure 3**]. This process of rapid winter ice growth over thin ice regions represents a
435 negative feedback, allowing for ice to form quickly over large parts of the Arctic Ocean
436 following summers with reduced ice cover and thinner November ice.
437   Thus, while summer sea ice is rapidly declining, several studies have indicated negative
438 feedbacks over winter continue to dominate [e.g. *Notz and Marotzke*, 2012; *Stroeve and Notz*,
439 2015], allowing for recovery following summers with anomalously low sea ice extent, such as
440 those observed in 2007 and 2012. This is further supported in the CICE-free simulations which
441 show the least amount of winter ice growth for the Arctic Basin in 1989, and peak ice growth
442 following the 2007 and 2012 record minimum sea ice extent [**Figure 9**]. As a result, mean ice
443 growth from November to April in CICE simulations from 1985 to 2017 shows a positive trend
444 that is weakly correlated to winter air temperatures or FDDs (*R=0.49*). On the other hand, we
445 find a strong inverse correlation (*R=-0.82*) between November sea ice thickness and winter ice
446 growth. Thus, because thin ice grows faster than thick ice, there is an overall stabilizing effect
447 that suggests as long as air temperatures remain below freezing, even if they are anomalously
448 warm, the ice can recover during winter. This stabilizing feedback over winter means that major
449 departures of the September sea ice extent from the long-term trend caused by summer
450 atmospheric variability generally does not persist for more than a few years [*Serreze and*
451 *Stroeve*, 2015].
452   However, since 2012, overall ice growth has declined as winter air temperatures have
453 increased further. This not surprising in that there was a lot of new ice to form in the open waters
454 left after the 2012 record minima. However, 2016 tied with 2007 for the second lowest Arctic sea
455 ice minimum and overall thermodynamic ice growth was significantly less. The correlation from
456 1985 to 2012 is smaller than over the full record (*R=0.34*), suggesting a growing influence of
457 warmer winter air temperatures though the difference in correlation is not statistically significant.
458 While there remains a large amount of inter-annual variability in winter warming events,

459   *Graham et al.* [2017] suggest a positive trend in not only the maximum temperature of these
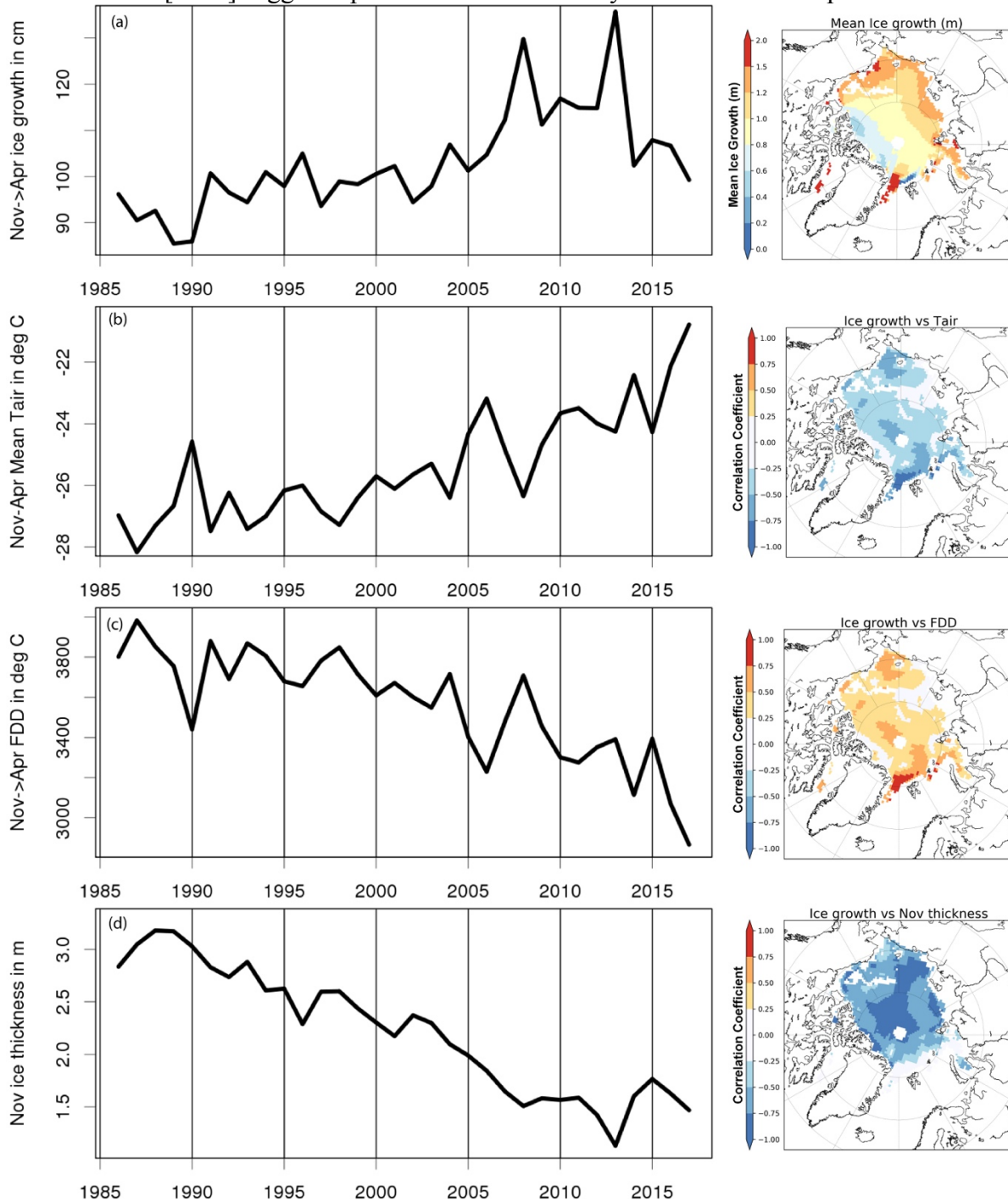
460
461 **Figure 9.** Time-series from 1985 to 2017 of mean winter ice growth (mid-November to mid-April) in the free CICE
462 simulation (a), mean 2m NCEP-2 air temperature (b), cumulative freezing degree days (FDDs) (c) and November ice
463 thickness (d). All time-series results are averaged over the areas shown in Figure S1(c). Corresponding images to
464 the left of each time-series plots show: mean ice growth from November to April as averaged from 1985/1986 to
465 2016/2017; correlation coefficient between ice growth and 2m NCEP-2 air temperature; correlation coefficient
466 between ice growth and FDDs; and correlation coefficient between ice growth and November ice thickness,
467 respectively. All correlation values are given for linear regression of de-trended time series.

468   warming events, but also in their duration. Interestingly, there is a modest correlation between
469   detrended FDDs and the winter maxima sea ice extent (*R=0.30*); not removing the trend results
470   in a correlation of *R=0.83*. Thus, recent reductions in overall FDDs may have played a role in the
471   last three years of record low maxima extents.
472
473   **Discussion**
474   The CICE-simulations and CS2 thickness retrievals from CPOM and AWI show consistency
475   that the Arctic Basin sea ice cover in April 2017 was on average 13 cm thinner than the 2011-
476   2017 mean. However, it may not have been the thinnest during the CS2 data record. Thickness
477   retrievals from the different CS2 data sets showed larger negative thickness anomalies in April
478   2013, ranging from -13 to -25 cm, whereas the CICE simulations showed smaller anomalies (-3
479   to -12 cm). While we expect retrievals from satellite to be more accurate than those from model
480   simulations, whether or not a year is anomalously low relative to another year will depend in part
481   on the inter-annual variability in the snow cover. All three CS2 products rely on the *W99* snow
482   depth climatology. While *Haas et al.* (2017) found snow depth within the Lincoln Sea in 2017
483   was similar to *W99*, evaluation of reanalysis data shows considerable variability in total
484   precipitation from year to year [*Barrett et al.*, submitted]. In the CICE-free simulations, snow
485   depth is modeled using precipitation from NCEP-2. Inter-annual variability from April 2011 to
486   April 2017 (calculated as standard deviation between the 7 monthly April means) is shown in
487   **Figure 10**. North of the CAA, standard deviations in snow depth are on the order of 12 to 14 cm,
488   whereas other regions are on the order of 2 to 12 cm. From the *W99* climatology, inter-annual
489   variability in snow depth during the winter months was estimated to be only 4 to 6 cm,
490   significantly less than what is exhibited here. Since ice thickness increases approximately 6 times
491   the snow depth uncertainty, a 12 to 14 cm uncertainty would lead to 72 to 83 cm change in CS2-
492   derived ice thickness. If we average for the area shown in Figure 1(d), snow depth anomalies
493   ranged from -6 cm to +6 cm, with a corresponding impact of -41 to +41 cm on thickness.
494
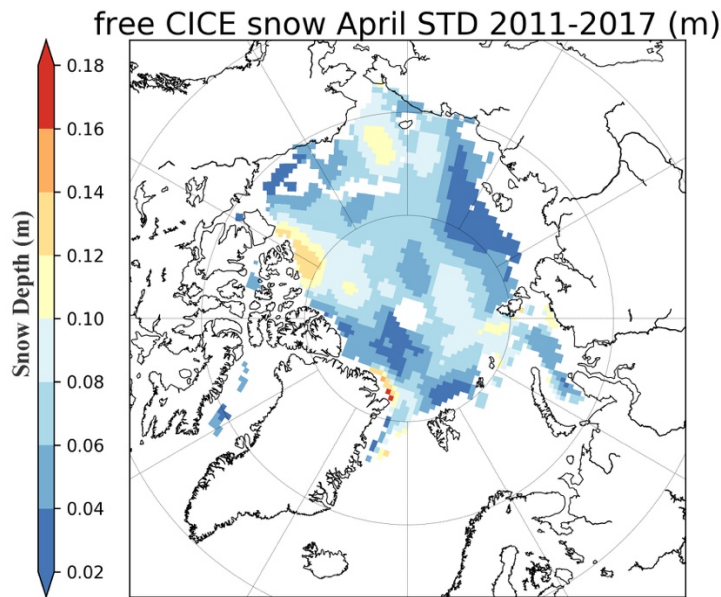
495
496   **Figure 10.** Standard deviation of CICE-simulated snow depth using NCEP-2 reanalysis for the month of April from
497   2011 to 2017.
498
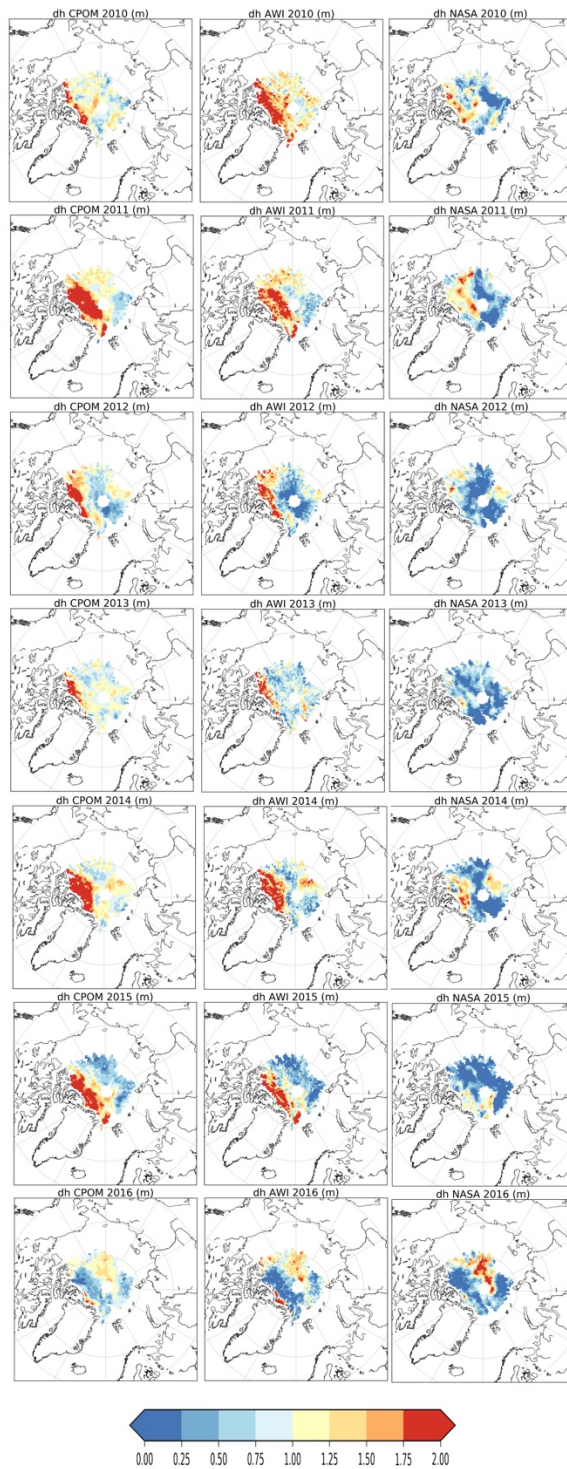
499
500   **Figure 11**. Comparison between ice growth (April minus November) in the UCL CPOM CryoSat-2 thickness
501   retrievals (left) and those from the Alfred Wegener Institute (AWI) (middle) and NASA (right). The year shown
502   corresponds to the November months, such that 2016 refers to ice thickness differences between April 2017 and
503   November 2016. Results are only shown for the area shown in Figure 1(c), which represents grid points that had
504   more than 100 individual measurements and a mean sea ice thickness greater than 0.5 m during the November
505   months.

506
507 Besides not accounting for inter-annual variability in snow depth, which makes assessing
508 thickness anomalies from one year to the next less certain, differences in waveform processing
509 between the three different CS2 products adds further uncertainty. The fact that the NASA CS2
510 product is a general outlier compared to the AWI and CPOM products is further highlighted in
511 **Figure 11**. Across the area considered (e.g. areas in color shown in Figure 1(c)), the difference
512 between April and the previous November ice thickness is shown for each CryoSat-2 year. The
513 AWI and CPOM products tend to exhibit positive ice growth over winter, focused north of
514 Greenland and the CAA and sometimes also across the pole. The NASA product on the other
515 hand generally shows less ice growth between November and April in most years, and even no
516 ice growth in some regions. The reasons for this are unclear, yet interestingly in winter
517 2016/2017, all three products show more agreement in regards to thickness decreases that span a
518 broad region north of Greenland and the CAA, combined with positive increases south of the
519 pole towards the East Siberian and Laptev seas.
520   Finally, how important were the April thickness anomalies in the evolution of the summer ice
521 cover in summer 2017? Several studies have discussed how thin winter ice may precondition the
522 Arctic for less sea ice at the end of the melt season as thinner ice melts and open water areas
523 form more readily in summer, enhancing the ice albedo feedback [e.g. *Stroeve et al.*, 2012;
524 *Perovich et al.*, 2008], and sea ice thickness has been used as a predictor for the September sea
525 ice extent [*Kimura et al.,* 2013]. Thus, we may have expected 2017 to be among the lowest
526 recorded sea ice extents as the ice cover was likely thinner than average and the winter extent
527 was the lowest in the satellite record. Nevertheless, the minimum extent ended up as the 8th
528 lowest in the satellite data record. This highlights the continuing importance of summer weather
529 patterns in driving the September minimum. Spring and summer 2017 were dominated by
530 several cold core cyclones, leading to near average air temperatures and ice divergence [see
531 http://nsidc.org/arcticseaicenews/ for a discussion of this summer's weather patterns]. Overall,
532 the correlation between detrended winter sea ice thickness anomalies and September sea ice
533 extent remains low [*Stroeve and Notz*, 2015]. Other factors such as melt pond formation in
534 spring [*Schröder et al.*, 2014] and summer weather patterns still largely govern the evolution of
535 the summer ice pack at current thickness levels [e.g. *Holland and Stroeve*, 2011]. Interestingly,
536 predictions of the monthly mean September 2017 sea ice extent based on spring melt pond
537 fraction in May gave a value of 5.0 ± 0.5 million km^2, whereas the observed value was 4.80
538 million km^2 [See arcus.org/sipn/sea-ice-outlook/2017/june].
539

540 **Conclusions**
541   In this study we examined sea ice thickness anomalies derived from three different CS2 data
542 products and that simulated using CICE. Overall freezing degree days were much reduced in
543 winter 2016/2017, and subsequent sea ice thickness estimates from CryoSat-2 in April 2017
544 suggest the ice was thinner over large parts of the Arctic Ocean. These results are complimented
545 with CICE model simulations, both with and without initializing with November ice thickness
546 distributions from CS2. While CICE simulations suggest the mean thickness within the Arctic
547 Basin in April 2017 was the thinnest over the CryoSat-2 data record, corresponding CS2-derived
548 sea ice thickness from the three different data providers put this into question. However, the use
549 of CS2-derived freeboards with a snow depth climatology remains problematic because it fails to
550 capture inter-annual snow accumulation variability. Differences in processing of the radar
551 waveform, values of snow and ice density, delineation of first-year vs. multiyear ice, and sea

552 surface height retrieval also contribute to differences among available data sets, making it
553 challenging to robustly assess inter-annual variability of ice thickness from CryoSat-2. Despite
554 these challenges it is encouraging that in most years, the interannual variability in positive and
555 negative anomalies is consistent between the 3 CS2 data sets.
556   Finally, CICE-free simulations from 1985 to 2017 reveal the correlation between winter ice
557 growth and November ice thickness ($R=-0.82$) is stronger than between growth and FDDs
558 ($R=0.49$), highlighting the importance of the negative winter growth feedback mechanism. This
559 supports previous studies that the long-term sea ice reduction in the Arctic Basin is mainly
560 driven by summer atmospheric conditions. However, this correlation has become weaker since
561 2012, indicating that higher winter air temperatures and further delays in autumn/winter freeze-
562 up due to warmer mixed-layer ocean temperatures prohibit a complete recovery of winter ice
563 thickness in spite of the negative feedback mechanism. This is highlighted by the fact that overall
564 thermodynamic ice growth for winter 2016/2017 was just under 1m despite 2016 reaching the
565 second lowest minimum extent recorded during the satellite record.
566

567 **Acknowledgements**
568 This work was in part funded under NASA grant NNX16AJ92G (Stroeve). Sea ice simulations
569 and CryoSat-2 satellite data processing performed under NERC funding of the Centre for Polar
570 Observation and Modeling (CPOM). CryoSat-2 thickness fields courtesy of A. Ridout at CPOM.
571 Processing of the AWI CryoSat-2 (PARAMETER) is funded by the German Ministry of
572 Economics Affairs and Energy (grant: 50EE1008) and data from November 2010 to April 2017
573 obtained from http://www.meereisportal.de (grant: REKLIM-2013-04). NASA CryoSat-2 data
574 provided courtesy of Nathan Kurtz. NCEP2 data obtained from NOAA Earth System Research
575 Laboratory (http://www.esrl.noaa.gov/psd/data/gridded/data.ncep.reanalysis2.gaussian.html).
576 Freeze-up data are available at https://neptune.gsfc.nasa.gov/csb/index.php?section=54. CICE
577 model output data available upon request.

578

579 **References**
580 Bekryaev, R.V., I.V. Polyakov and V.A. Alexeev (2010), Role of polar amplification in long-
581   term surface air temperature variations and modern Arctic warming, *J. Clim*, 23, 3888-3906.
582 Bitz, C.M. and G.H. Roe (2004), A mechanism for the high rate of sea ice thinning in the Arctic
583   Ocean, *J. Clim*. 17, 2623-2632, doi:10.1175/1520-0442(2004)017<3623:AMFTHR>2.0CO;2.
584 Boisvert, L.N., A.A. Petty, and J. Stroeve (2016), The Impact of the Extreme Winter 2015/16
585   Arctic Cyclone on the Barents–Kara Seas, *Bull. Amer. Met. Soc.*, doi:10.1175/MWR-D-16-
586   0234.1.
587 Cohen, L., S. R. Hudson, V. P. Walden, R. M. Graham, M. A. Granskog (2017), Meteorological
588   conditions in a thinner Arctic sea ice regime from winter through early summer during the
589   388 Norwegian young sea ICE expedition (N-ICE2015), *J. Geophys. Res. Atmos.*,
590   doi:10.1002/2016JD026034.
591 Cullather, R. I., Y. Lim, L. N. Boisvert, L. Brucker, J. N. Lee, and S. M. J. Nowicki (2016),
592   Analysis of the 426 warmest Arctic winter, 2015-2016, *Geophys. Res. Lett.*, 808–816,
593   doi:10.1002/2016GL071228.
594 Dee, D. P. et al. (2011), The ERA-Interim reanalysis: Configuration and performance of the data
595   428 assimilation system, *Q. J. R. Meteorol. Soc.*, 137(656), 553–597, doi:10.1002/qj.828.
596 Flocco, D., D. Schröder, D. L. Feltham, and E. C. Hunke (2012), Impact of melt ponds on Arctic
597   sea ice simulations from 1990 to 2007, *J. Geophys. Res.*, doi:10.1029/2012JC008195.

Graham, R.M., L. Cohen, A.A. Petty, L.N. Boisvert, A. Rinke, S.R. Hudson, M. Nicolaus and M.A. Granskog, (2017), increasing frequency and duration of Arctic winter warming events, *Geophys. Res. Lett.*, 16, 6974-6983, doi:10.1002/2017GL073395.

Graversen, R.G. and M. Burtu (2016), Arctic amplification enhanced by latent energy transport of atmospheric planetary waves, *Quart. Royal Meteoro. Soc.*, doi:10.1002/qj.2802.

Graversen RG. 2006. Do changes in midlatitude circulation have any impact on the Arctic surface air temperature trend? *J. Clim.* **19**: 5422–5438.

Haas, C., Beckers, J., King, J., Silis, A., Stroeve, J., Wilkinson, J., Notenboom, B., Schweiger, A., & Hendricks, S. (2017). Ice and snow thickness variability and change in the high Arctic Ocean observed by in situ measurements. *Geophys. Res. Lett*, 44, 10,462–10,469, doi:10.1002/2017GL075434.

Hendricks, S., R. Ricker and V. Helm (2016), User Guide - AWI CryoSat-2 Sea Ice Thickness Data Product (v1.2).

Holland, M.M. and J.C. Stroeve (2011), Changing seasonal sea ice predictor relationships in a changing Arctic climate, Geophys. Res. Lett., doi:10.1029/2011GL049303.

Hunke, E. C., W. H. Lipscomb, A. K. Turner, N. Jeffery, and S. Elliott (2015), CICE: the Los Alamos Sea Ice Model Documentation and Software User's Manual Version 5.1.

Jakobshavn, E., T. Vihma, T. Palo, L. Jakobson, H. Keernik and J. Jaagus (2012), validation of atmospheric reanalysis over the central Arctic Ocean, *Geophys. Res. Lett.*, 39, L10802, doi:10.1029/2012GL051591.

Kanamitsu, M., W. Ebisuzaki, J. Woollen, S-K Yang, J.J. Hnilo, M. Fiorino, and G. L. Potter (2002, updated 2017), NCEP-DOE AMIP-II Reanalysis (R-2): 1631-1643, *Bull. Amer. Met. Soc*.

Kimura, N., A. Nishimura, Y. Tanaka and H. Yamaguchi (2013), Influence of winter sea-ice motion on summer ice cover in the Arctic, *Polar Research*, 32, doi:10.3402/polar.v32i0.20193.

Kurtz, N. and J. Harbeck. 2017. *CryoSat-2 Level 4 Sea Ice Elevation, Freeboard, and Thickness, Version 1*. [Indicate subset used]. Boulder, Colorado USA. NASA National Snow and Ice Data Center Distributed Active Archive Center. [Date Accessed].

Kurtz, N.T., N. Galin and M. Studinger (2014), An improved CryoSat-2 sea ice freeboard retrieval algorithm through the use of a waveform fitting, The Cryosphere, 8, 1217-1237, doi:10.5194/tc-802017-2014.

Kwok, R. (2015), Sea ice convergence along the Arctic coasts of Greenland and the Canadian Arctic Archipelago: Variability and extremes (1992–2014), *Geophys. Res. Lett.*, 42, 7598–7605, doi:10.1002/2015GL065462.

Laxon, S. W., K.A. Giles, A.L. Ridout, D.J. Wingham, R. Willatt, R. Cullen, R. Kwok, A. Schweiger, J. Zhang, C. Haas, S. Hendricks, R. Krishfield, N. Kurtz, S. Farrell, and M. Davidson, (2013), CryoSat-2 estimates of Arctic sea ice thickness and volume, *Geophys. Res. Lett.*, 40, 732–737, doi:10.1002/grl.50193.

Markus, T., J. C. Stroeve, and J. Miller, (2009). Recent changes in Arctic sea ice melt onset, freeze-up, and melt season length, *J. Geophys. Res.*, doi:10.1029/2009JC005436.

Merkouriadi, I., B. Cheng, R.M. Graham, A. Rosel and M.A. Granskog (2017), Critical role of snow on sea ice growth in the Atlantic sector of the Arctic Ocean, *Geophysical Research Letters*, 44, 10-479-10,485, doi:10.1002/2017GL075494.

Moore, G. W. K. (2016), The December 2015 North Pole Warming Event and the Increasing 457 Occurrence of Such Events, *Sci. Rep.*, 6(November), 39084, doi:10.1038/srep39084.

644 Moore, G. W. K., Schweiger, A., Zhang, J. & Steele, M. (2018), Collapse of the 2017 winter
645   Beaufort High: A response to thinning sea ice?, *Geophys. Res. Lett.*, 45.
646   Doi:10.1002/2017GL076446.
647 Notz, D. and J. Marotzke (2012), Observations reveal external driver for Arctic sea ice retreat,
648   *Geophys. Res. Lett.*, doi:10.1029/2012GL051094.
649 Overland, J. E., and M. Wang (2016), Recent extreme arctic temperatures are due to a split polar
650   vortex, *J. Clim.*, 29(15), 5609–5616, doi:10.1175/JCLI-D-16- 0320.1.
651 Perovich, D.K., J.A. Richter-Menge, K.F. Jones and B. Light (2008), Sunlight, water and ice:
652   Extreme Arctic sea ice melt during the summer of 2007, *Geophys. Res. Lett.*,
653   doi:10.1029/2008GL034007.
654 Pithan, F. and T. Mauritsen (2014), Arctic amplification dominated by temperature feedbacks in
655   contemporary climate models, *Nature Geoscience*, 7, 181-184, doi:10.1038/ngeo2017.
656 Polyakov I.V., A. Beszczynska, E.C. Carmack, I.A. Dmitrenko, E. Fahrbach, I.E. Frolov, R.
657   Gerdes, E. Hansen, J. Holfort, V.V. Ivanov, M.A. Johnson, M. Karcher, F. Kauker, J.
658   Morison, K.A. Orvik, U. Schauer, H.L. Simmons, A. Skagseth, V.T. Sokolov, M. Steele, L.A.
659   Timokhov, D. Walsh and J.E. Walsh (2005), One more step towards a warmer
660   Arctic. *Geophys. Res. Lett.* 32, L17605, doi: 10.1029/2005GL023740.
661 Rae, J.G.L., H.T. Hewitt, A.B. Keen, J.K. Ridley, J.M. Edwards, and C.M. Harris (2014), A
662   sensitivity study of the sea ice simulation in HadGEM3, *Ocean Model*. 74, 60–76,
663   doi:10.1016/j.ocemod.2013.12.003.
664 Ricker, R., S. Hendricks, F. Girard-Ardhuin, L. Kaleschke, C. Lique, X. Tian-Kunze, M.
665   Nicolaus, and T. Krumpen (2017a), Satellite observed drop of Arctic sea ice growth in winter
666   2015-2015, *Geophys. Res. Lett.*, doi:10.1002/2016GL072244.
667 Ricker, R., S. Hendricks, L. Kaleschke, X. Tian-Kunze, J. King and C. Haas (2017b), A weekly
668   arctic sea-ice thickness data record from merged cryosat-2 and SMOS satellite data, *The*
669   *Cryosphere*, 1-27, doi:10.5194/tc-2017-4.
670 Ricker, R., S. Hendricks, V. Helm, H. Skourup, and M. Davidson (2014a), Sensitivity of
671   CryoSat-2 Arctic sea-ice freeboard and thickness on radar-waveform interpretation, *The*
672   *Cryosphere*, 8 (4), 1607-1622, doi:10.5194/tc-8-1607-2014.
673 Rigor, I.G., J.M. Wallace and R.L. Colony (2002), Response of sea ice to the Arctic Oscillation,
674   *J. Clim.*, doi:10.1175/1520-0442(2002)015<2648:ROSITT>2.0.CO;2.
675 Schröder D., D. L. Feltham, D. Flocco, M. Tsamados (2014), September Arctic sea-ice minimum
676   predicted by spring melt-pond fraction. *Nature Clim. Change*, doi 10.1038/NCLIMATE2203.
677 Screen, J.A and I. Simmonds (2010), The central role of diminishing sea ice in recent Arctic
678   temperature amplification, *Nature*, 464, 1334-1337.
679 Serreze, M.C., A.P. Barrett, J.C. Stroeve, D.M. Kindig, M.M. Holland (2009), The emergence of
680   surface-based Arctic amplification, *The Cryosphere*, 3, pp. 11–19.
681 Stroeve, J. and D. Notz (2015), Insights on past and future sea-ice evolution from combining
682   observations and models, *Global and Planetary Change*, doi:10.1016/gloplacha.2015.10.011.
683 Stroeve, J.C., T. Markus, L. Boisvert, J. Miller and A. Barrett (2014), Changes in Arctic Melt
684   Season and Implications for Sea Ice Loss. Geophysical Research Letters,
685   doi:10.1002/2013GL058951.
686 Stroeve, J.C., M.C. Serreze, J.E. Kay, M.M. Holland, W.N. Meier and A.P. Barrett, (2012). The
687   Arctic's rapidly shrinking sea ice cover: A research synthesis, *Clim. Change*, doi:
688   10.1007/s10584-011-0101-1.
689 Tilling, R. L., A. Ridout, A. Shepherd, and D. J. Wingham (2015), Increased arctic sea 454 ice

690   volume after anomalously low melting in 2013, *Nature Geoscience*, 8 (8), 643–646.

691 Tilling, R. L., A. Ridout and A. Shepherd (2016), Tilling, R. L., A. Ridout, and A. Shepherd,

692   Near-real-time Arctic sea ice thickness and volume from CryoSat-2, *The Cryosphere*, 10,

693   doi:10.5194/tc-10-2003-2016.

694 Tilling, R.L., A. Ridout, and A. Shepherd (2017), Estimating Arctic sea ice thickness and volume

695   using CryoSat-2 radar altimeter data, *Advances in Space Research*,

696   doi:10.1016/j.asr.2017.10.051.

697 Tsamados M., D. L. Feltham, D. Schröder, D. Flocco, S. Farrell, N. Kurtz, S.Laxon, and S.

698   Bacon (2014), Impact of variable atmospheric and oceanic form drag on simulations of Arctic

699   sea ice. *J. Phys. Oceanogr*. 44 (1329-1353), doi:10.1175/JPO-D-13-0215.1.

700 Tsamados, M., D. Feltham, A. Petty, D. Schröder and D. Flocco (2015), Processes controlling

701   surface, bottom and lateral melt of Arctic sea ice in a state of the art sea ice model, *Phil.*

702   *Trans. R. Soc. A* 373.2052, doi:10.1098/rsta.2014.0167.

703 Warren, S.G., I.G. Rigor, N. Untersteiner, V.F. Radionov, N.N. Bryazgin, Y.I. Aleksandrov and

704   R. Barry (1999), Snow depth on Arctic sea ice, J. Clim., 12, 1814-1829.

705 Willatt, R., S. Laxon, K. Giles, R. Cullen, C. Haas, and V. Helm (2011), Ku-band radar

706   penetration into snow cover Arctic sea ice using airborne data, *Ann. Glaciol.*, **52**(57), 197–

707   205.

708

709

710

711

712 **Table 1**. Regional trends in freeze-up, 2017 freeze-up date and anomaly (relative to 1981-2010
713 mean). Freeze-up is computed following Markus et al. (2009).

Region	Freeze-up Trend (days per decade)	2017 Mean Freeze-up (day of year)	2017 Freeze-up Anomaly (days)
Sea of Okhotsk	9.1	304	0.8
Bering Sea	6.7	338	25.2
Hudson Bay	7.9	333	16.9
Baffin Bay	8.0	312	13.2
E. Greenland Sea	5.6	267	2.7
Barents Sea	13.6	347	60.3
Kara Sea	10.7	314	36.6
Laptev Sea	9.0	272	10.7
E. Siberian Sea	11.8	286	27.1
Chukchi Sea	14.1	314	31.0
Beaufort Sea	8.9	279	23.4
Canadian Archipelago	4.9	268	12.7
Central Arctic	3.1	255	16.8
Pan-Arctic	7.5	288	19.6

714

715 **Table 2.** Mean November ice thickness and anomaly with respect to the 2011-2017 mean (in
716 parenthesis) from CS2 derived from CPOM, AWI and NASA. Spatial mean is over Arctic Basin,
717 defined as the area for which CS-data were available continuously for all 7 winter periods
718 November to April 2010/2011 to 2016/17. This region corresponds to all three regions shown in
719 Figure 1(c).

	November SIT CS2 CPOM (cm)	November SIT CS2 AWI (cm)	November SIT CS2 NASA (cm)	November SIT CICE-free (cm)
2010	183 (-6)	208 (-8)	198 (-7)	206 (+6)
2011	157 (-32)	174 (-42)	170 (-35)	185 (-15)
2012	173 (-16)	192 (-24)	177 (-28)	152 (-48)
2013	212 (+23)	246 (+29)	243 (+38)	208 (+08)
2014	207 (+18)	239 (+23)	226 (+21)	231 (+31)
2015	196 (+7)	229 (+13)	217 (+12)	219 (+19)
2016	193 (+4)	225 (+9)	204 (-1)	199 (-1)
2010-2016 mean	189	216	205	200

720
721

722

723
724
725

726 **Table 3.** Mean April sea ice thickness (SIT) and anomaly with respect to the 2011-2017 mean (in
727 parenthesis) from three CS2 products (CPOM, AWI and NASA), and the CICE (free run 1985-
728 2017) and CICE runs initialized with CS2 ice thickness in November. The amount of
729 thermodynamic ice growth and dynamical ice change from the CICE model runs is also given.
730 Spatial mean is over Arctic Basin, defined as the area shown in Figure 1(d).

731

	CryoSat-2 Results			CICE Simulations					
	April SIT CPOM (cm)	April SIT AWI (cm)	April SIT (NASA) (cm)	April SIT CICE free (cm)	April SIT CICE ini (cm)	Therm growth CICE free (cm)	Therm growth CICE ini (cm)	Dyn change CICE free (cm)	Dyn change CICE ini (cm)
1990-2017 Mean	n/a	n/a	n/a	283	n/a	107	n/a	-18	n/a
2010-2017 Mean	243	230	235	246	240	112	103	-15	-17
2011	239 (-4)	237 (+7)	227 (-8)	242 (-4)	241 (+1)	115 (+3)	104 (+1)	-18 (-3)	-20 (-3)
2012	235 (-8)	219 (-11)	218 (-17)	247 (+1)	233 (-7)	115 (+3)	110 (+7)	-9 (+6)	-12 (+5)
2013	230 (-13)	208 (-22)	210 (-25)	234 (-12)	237 (-3)	136 (+24)	117 (+14)	-16 (+1)	-19 (-2)
2014	261 (+18)	250 (+20)	254 (+19)	251 (+5)	249 (+9)	102 (-10)	94 (-9)	-12 (+3)	-17 (+0)
2015	264 (+21)	252 (+22)	254 (+19)	264 (+18)	255 (+11)	108 (-4)	103 (-0)	-18 (-3)	-22 (-5)
2016	239 (-4)	227 (-3)	228 (-7)	254 (+8)	241 (+1)	107 (-5)	101 (-2)	-15 (-0)	-17 (+0)
2017	230 (-13)	218 (-12)	238 (+3)	233 (-13)	227 (-13)	99 (-13)	92 (-11)	-14 (+1)	-13 (+4)

732
733

734

735